Complex-valued time-series correlation increases sensitivity in FMRI analysis

Mary C. Kociuba [a], Daniel B. Rowe [a,b,*]

[a] Department of Mathematics, Statistics, and Computer Science, Marquette University, Milwaukee, WI, USA
[b] Department of Biophysics, Medical College of Wisconsin, Milwaukee, WI, USA

ARTICLE INFO

ABSTRACT

Purpose: To develop a linear matrix representation of correlation between complex-valued (CV) time-series in the temporal Fourier frequency domain, and demonstrate its increased sensitivity over correlation between magnitude-only (MO) time-series in functional MRI (fMRI) analysis.

Materials and methods: The standard in fMRI is to discard the phase before the statistical analysis of the data, despite evidence of task related change in the phase time-series. With a real-valued isomorphism representation of Fourier reconstruction, correlation is computed in the temporal frequency domain with CV time-series data, rather than with the standard of MO data. A MATLAB simulation compares the Fisher-*z* transform of MO and CV correlations for varying degrees of task related magnitude and phase amplitude change in the time-series. The increased sensitivity of the complex-valued Fourier representation of correlation is also demonstrated with experimental human data. Since the correlation description in the temporal frequency domain is represented as a summation of second order temporal frequencies, the correlation is easily divided into experimentally relevant frequency bands for each voxel's temporal frequency spectrum. The MO and CV correlations for the experimental human data are analyzed for four voxels of interest (VOIs) to show the framework with high and low contrast-to-noise ratios in the motor cortex and the supplementary motor cortex.

Results: The simulation demonstrates the increased strength of CV correlations over MO correlations for low magnitude contrast-to-noise time-series. In the experimental human data, the MO correlation maps are noisier than the CV maps, and it is more difficult to distinguish the motor cortex in the MO correlation maps after spatial processing.

Conclusions: Including both magnitude and phase in the spatial correlation computations more accurately defines the correlated left and right motor cortices. Sensitivity in correlation analysis is important to preserve the signal of interest in fMRI data sets with high noise variance, and avoid excessive processing induced correlation.

© 2016 Elsevier Inc. All rights reserved.

1. Introduction

In fMRI, the measured blood oxygen level dependent (BOLD) signal to detect neural activity is spatially Fourier encoded [1,2]. The BOLD fluctuations are measured as a complex-valued fMRI signal over time in the spatial frequency domain, then the *k*-space readout is reconstructed with the inverse Fourier transform (IFT). Before the statistical analysis of the fMRI data, the phase portion of the data is generally discarded, despite physiologically useful information contained in the phase [3]. Previous research suggests that phase-only change arises from large draining vessels [4], or proposes

methods to filter phase signal contributions from large vessels [4,5]. Although, other models support the notion that randomly oriented vasculature yield phase change in fMRI studies [6,7]. It has been previously demonstrated that modeling an fMRI time-series with both magnitude and phase increases the power of the activation statistics [8–11] over those from MO models. This manuscript outlines a method to describe correlation between two time-series with both magnitude and phase (equivalently real and imaginary), through exploiting the linear relationship between the image domain and spatial frequency domain. Traditionally both MO and CV models require analysis in the image domain, however, analysis within the frequency domain is also valuable. It has previously been shown how complex-valued temporal frequencies contribute to the correlations between voxels in the cerebral cortex for magnitude-only non-task data [12]. Similarly, in this manuscript the spatial correlation between complex-valued time series is described as a

* Corresponding author at: Department of Mathematics, Statistics, and Computer Science, Marquette University, Milwaukee, WI, USA. Tel.: +1 414 288 5228; fax: +1 414 288 5472.

E-mail addresses: daniel.rowe@marquette.edu, dbrowe@mcw.edu (D.B. Rowe).

linear combination of second order voxel temporal frequencies. The present study advances the frequency correlation description into a linear matrix framework with an application to a complex-valued simulation demonstrating the strength of the model at low magnitude and phase contrast-to-noise ratio (CNR) values, as well demonstrating its utility in experimental complex-valued fMRI data.

During signal acquisition, unwanted image acquisition artifacts and physiological noise obscure the true underlying signal of interest. To improve the signal-to-noise ratio (SNR), various preprocessing operations, *i.e.* temporal frequency filtering or magnitude image smoothing, are incorporated in the processing and reconstruction pipeline, and physiologic noise sources are commonly regressed out from the signal [13–16]. It is well documented that the application of these operations induces local spatial and temporal correlations into neural regions that were previously uncorrelated [17–19]. The linear framework developed in this manuscript also describes how signal processing alters the structure of the spatial covariance matrix, such that induced correlation is a result of increased overlapping frequency content between voxels after processing. Signal processing will alter the activated voxel's temporal frequency spectrums, by spreading voxel task activated peaks temporally and spatially. Correlation will be induced between voxels as a result of increased overlapping frequency content between the two voxel's Fourier frequency spectrums. This notation for spatial correlation is advantageous since various physiological signals are also confined to specific frequency ranges. Respiratory and cardiac cycle fluctuations are characterized around 0.2–0.3 Hz and 1 Hz in a voxel's temporal frequency spectrum, although they are often aliased to low frequencies in fMRI signal acquisition [13,20,21]. The summation notation of spatial correlation that is described here, allows relative contributions to the correlation to be quantified by segregating the natural partitions in a voxel's temporal frequency spectrum. Compared to magnitude-only correlations, applying this framework with complex-valued data more accurately identifies regions of spatial correlation, and reduces the false positives in correlation maps. This result is most significant in low magnitude CNR data sets since including the phase in the complex-valued correlation results in increased sensitivity of identifying correlated regions.

2. Theory

A $p_{row} \times p_{col}$ complex-valued k-space readout is reconstructed to a single image with the discrete inverse Fourier transform (IFT). With a real-valued isomorphism representation [22] of the Fourier reconstruction operator, Ω, and the k-space readout in vector form, s_t, an image vector, y_t, for a single image time point, t, is reconstructed as

$$y_t = \Omega s_t. \tag{1}$$

Equivalently, with the forward Fourier Transform $\Omega^{-1} = \overline{\Omega}$, the k-space readout is written as

$$s_t = \overline{\Omega} y_t. \tag{2}$$

In Eqs. (1) and (2), the signal and image vectors are $2p \times 1$, where $p = p_{row} p_{col}$ is the number of voxels, and the real parts are stacked over the imaginary parts, so $s_t = (s_R', s_I')'$ and $y_t = (y_R', y_I')'$. The real parts in each vector are organized as $s_R = (s_{R1},...,s_{Rp})'$ and $y_R = (y_{R1},...,y_{Rp})'$, and the imaginary parts in each vector are organized as $s_I = (s_{I1},...,s_{Ip})'$ and $y_I = (y_{I1},...,y_{Ip})'$. To build up the

real-valued matrix framework, consider the representation of the inverse Fourier reconstruction.

$$\Omega = \begin{bmatrix} \Omega_R & -\Omega_I \\ \Omega_I & \Omega_R \end{bmatrix}$$

where Ω_R and Ω_I are constructed with the Kronecker product, $\Omega_R = [(\Omega_{yR} \otimes \Omega_{xR}) - (\Omega_{yI} \otimes \Omega_{xI})]$

and $\Omega_I = [(\Omega_{yR} \otimes \Omega_{xI}) + (\Omega_{yI} \otimes \Omega_{xR})]$. The jkth element of the $p_{col} \times p_{col}$ Fourier matrix Ω_x is $(\Omega_x)_{jk} = w^{(-\frac{pcol}{2}+j)(-\frac{pcol}{2}+k)}$ where j and k have indexing values from 0 to $p_{col}-1$ with $w = \frac{1}{N}e^{i2\pi/p_{col}}$ for the IFT and $w = e^{-i2\pi/p_{col}}$ for the forward Fourier transform (FT), [22].

To reconstruct images over n time repetitions (TRs), the complex-valued spatial frequencies are represented in the real-valued $2pn \times 1$ vector s, with each successive TR concatenated to the vector. An analogous explanation describes the organization of the real-valued image $2pn \times 1$ vector, y, which is reconstructed with the Kronecker product,

$$y = (I_n \otimes \Omega)s. \tag{3}$$

A $2pn \times 2pn$ permutation matrix, P, reorders the elements of vector y so the real-valued time-series $2pn \times 1$ vector $v = Py$ is now ordered by voxel rather than ordered by image. The voxel ordered time-series is Fourier transformed into the temporal frequency domain, with the $2n \times 2n$ temporal forward Fourier transform (FT) matrix, Ω_T, as opposed to the $2p \times 2p$ spatial Fourier operations. The real-valued $2pn \times 1$ vector f consists of the temporal frequencies of each voxel stacked upon the corresponding imaginary temporal frequencies is represented,

$$f = \left(I_p \otimes \overline{\Omega}_T\right)Py. \tag{4}$$

For voxel α, the $2n \times 1$ real-valued voxel time-series is denoted v_α, with real parts stacked over imaginary parts $v_\alpha = (v_{\alpha R}', v_{\alpha I}')'$ so the real and imaginary parts in each vector are organized as $v_{\alpha R} = (v_{\alpha R1},...,v_{\alpha Rn})'$ and $v_{\alpha I} = (v_{\alpha I1},...,v_{\alpha In})'$, with a mean and covariance structure of $\mu_{R\alpha}$ and $\mu_{I\alpha}$, $\sigma^2_{R\alpha}I_n$ and $\sigma^2_{I\alpha}I_n$. The corresponding temporal frequencies for voxel α are denoted in the $2n \times 1$ vector f_α, where $v_\alpha = \Omega_T f_\alpha$ and $f_\alpha = \Omega_T v_\alpha$, are organized similarly to the time-series equivalent. With an analogous description of another voxel β, the spatial covariance between the two voxels is simply written, $cov(v_\alpha, v_\beta) = (v_\alpha - \mu_\alpha)^T(v_\beta - \mu_\beta)/(2n)$.

Assuming the time-series is demeaned, then the covariance between two voxels in terms of temporal frequencies is represented as,

$$cov\left(v_\alpha, v_\beta\right) = \left(v_\alpha^T v_\beta\right)/(2n) = \left(\overline{\Omega}_T f_\alpha\right)^T \left(\overline{\Omega}_T f_\beta\right) = \left(f_\alpha^T f_\beta\right)/4 \tag{5}$$

The spatial covariance in Eq. (5) is expanded to a $p \times p$ spatial covariance matrix, Σ, such that the entry (α, β) in Σ represents the spatial covariance between the two demeaned real-valued voxel time-series of voxel α and voxel β. By defining D as the diagonal matrix consisting of the diagonal elements of Σ, a $p \times p$ spatial correlation matrix is written as,

$$R = D^{-1/2} \Sigma D^{-1/2}. \tag{6}$$

By aggregating the second order temporal frequencies into biologically meaningful or experimentally relevant bands, the influence preprocessing steps have on each voxel temporal frequency spectrum can be quantitatively measured. In an fMRI study, the frequency corresponding to the activation is considered when dividing the spectrum into bands. To understand the contribution each temporal frequency band yields to spatial correlation, the

correlation is expressed as, the spatial covariance matrix can be written as a summation of covariance of each band and b is the total number of bands,

$$\Sigma = \Sigma_1 + \ldots + \Sigma_b,$$

and the Eq. (7) spatial correlation matrix can be written as a summation of correlation of bands

$$R = D^{-1/2}(\Sigma_1 + \ldots + \Sigma_b)D^{-1/2} = R_1 + \ldots + R_b. \tag{7}$$

Input of processing operations in the context of the Fourier framework is described in Appendix A.

3. Methods

3.1. Theoretical illustration

To demonstrate the improved strength of correlation between CV time-series over correlation between MO time series in functional MRI studies, a MATLAB simulation is run with a varying degree of magnitude contrast-to-noise ratio (CNR_ρ) and the phase contrast-to-noise ratio (CNR_ϕ). The SNR is defined as the baseline magnitude signal over the standard deviation of the noise in the time-series, $SNR = \rho/\sigma$. For the CNR, the amplitude is defined as the difference between the baseline signal and the task related change in the signal for the magnitude and phase components of the time-series, A_ρ and A_ϕ, so $CNR_\rho = A_\rho/\sigma$ and $CNR_\phi = A_\phi/(\sigma/\rho)$. Assuming normal noise in the real and imaginary channels, the standard deviation of a phase-only time-series is σ/ρ, and the CNR_ϕ is proportional to the SNR. Typically in fMRI studies, the task related signal change in the magnitude A_ρ corresponds to approximately a 1–2% signal change, and the task related change in the phase A_ϕ has been found to be approximately $\pi/36$ [4]. To compare MO and CV correlations, two 96×96 surfaces are generated with 720 time-points and standard normal random noise added to the real and imaginary channels. As visualized in Fig. 1, each voxel has a ρ between 0 and 50, and a task generated to represent a magnitude amplitude A_ρ between 0 and 1, and a phase amplitude A_ϕ between 0 and $\pi/36$. The MO and CV correlations are computed between the two time-series in each surface with equivalent parameter settings, so there is a 96×96 corresponding matrix for MO and CV. To compare the correlations between the two models, the Fisher-z transform, z, is computed and plotted for each time-series correlation, r, as

$$z = 1/2 \ln\left(\frac{1+r}{1-r}\right).$$

3.2. Experimental illustration

An experimental fMRI human data set is acquired with bilateral finger tapping, performed for sixteen 22-s periods, a block design experiment was acquired for a series of 720 TRs with a 3.0 T Discovery MR750 MRI scanner (General Electric, Milwaukee, WI) using a GE single channel quadrature head coil. The data set was acquired with ten interleaved 4 mm thick axial slices that are 96×96 in dimension for a 24.0 cm FOV, with a TR/TE of 1000/39 ms, a flip angle of 25°, and an acquisition bandwidth of 111 kHz. To observe the potential impact of data processing on the temporal frequencies and demonstrate the utility of the framework, voxel temporal spectrums are analyzed before and after applying a spatial smoothing operator with a Gaussian kernel with a full-width-half-max of 3 voxels, followed by an ideal high-pass band filter (<0.009 Hz) and low-pass band filter (>0.08 Hz). The spatial correlation is decomposed into three correlation bands, R_1, R_2, R_3, such that sum of the bands equals the total correlation. The correlation bands that are selected correspond to the frequency band ranges 0.0009–0.024 Hz, 0.026–0.037 Hz, 0.038–0.08 Hz, with the task-activated frequency peak is observed in R_2. The complex activation for the data was computed [9], and four voxels were chosen based on their complex activation locations: two in the motor cortex and two in the supplementary motor cortex. The two voxels in each location are chosen so that one voxel has a high CNR_ρ and CNR_ϕ, and the other has a low CNR_ρ and CNR_ϕ.

4. Results

4.1. Simulated data

In Fig. 2, the Fisher-z transform statistics for the MO and CV correlations are computed for the surfaces generated with the parameters described in Fig. 1. Including the phase half of the data in the CV correlation calculation yields an increased sensitivity of the correlation value, as illustrated by comparing the top left corner of the Fisher-z map in Fig. 2a to the one in Fig. 2b, with a difference map of CV–MO in Fig. 2c. The additional information of the phase time-series improves the strength of correlation detected at lower magnitude CNR values.

4.2. Experimental data

Figs. 3 and 4 contain the four seed voxel CV and MO spatial correlation maps for the experimental fMRI data in the motor cortex and supplementary motor cortex. In Fig. 3b, the MO and CV correlation maps are identical since computing the MO and CV correlations are equivalent for a MO data set. In Fig. 4b, the MO and
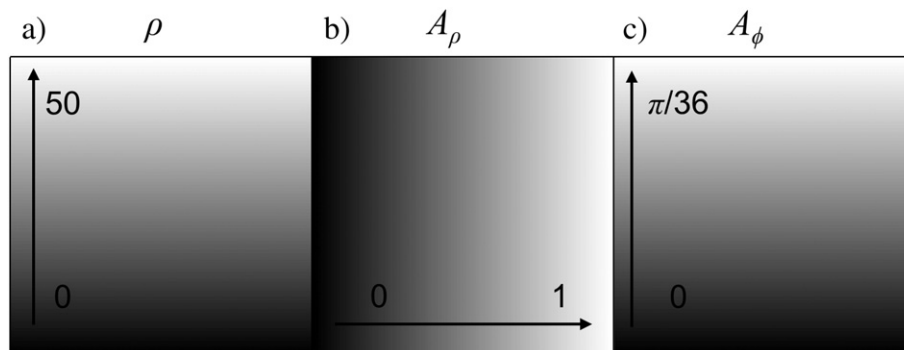
Fig. 1. Surfaces representing the (a) ρ, (b) A_ρ, and (c) A_ϕ parameters used to generate the simulated time-series.
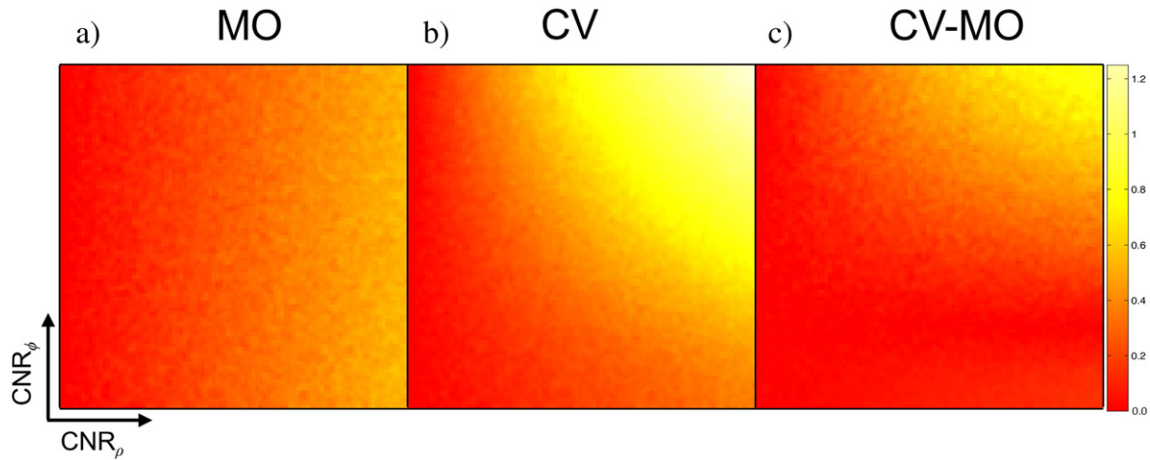
Fig. 2. The Fisher-*z* transform of the (a) MO and (b) CV correlation, and the (c) difference (CV–MO) between the correlations.

CV correlation maps are noticeably distinguishable since computing the MO and CV correlations are not equivalent for a CV data set. As described in Eq. (7), the spatial correlations are computed with the temporal frequencies, which are aggregated into bands as seen in Figs. 3a and 4a. The MO correlation maps appear to contain more correlations outside the expected task-activated region compared to the CV maps. Particularly in the low CNR seed voxels, the less defined motor cortex in the MO correlation maps corroborates the results observed in the simulation in Section 4.1. The CV correlations have a higher sensitivity than the MO correlations in both regions with activation. All voxels are located in the motor cortex or supplementary motor cortex, and exhibit task-activated correlation in R_2, where the task frequency peak is located, as in Figs. 3a and 4a. In Fig. 3b, the general location of the apparent false positive MO correlation is around the edge of the brain as is characteristic of a motion artifact.

Since the data has been minimally processed, motion artifacts are present in the data and have not been corrected.

5. Conclusions

A linear matrix representation of correlation between complex-valued time-series in the temporal Fourier frequency domain for functional MRI (fMRI) data analysis was developed. In a simulation comparing decreasing CNR magnitude and phase values, it was illustrated that the Fisher-*z* transform of CV correlations was higher than for MO correlations for low CNR fMRI time-series. In the experimental human data, a comparison of R_2 in Figs. 3a and 4a shows increased sensitivity of estimating correlations with including the phase time-series. These results agree with previous studies investigating the statistical power of using CV data over MO data in
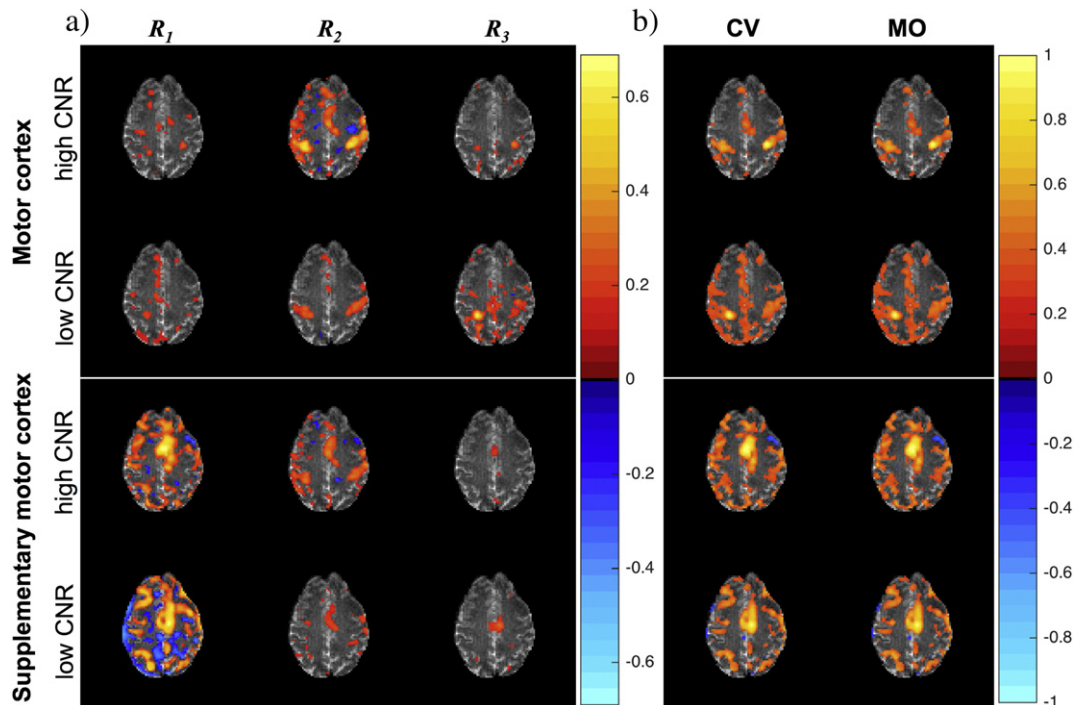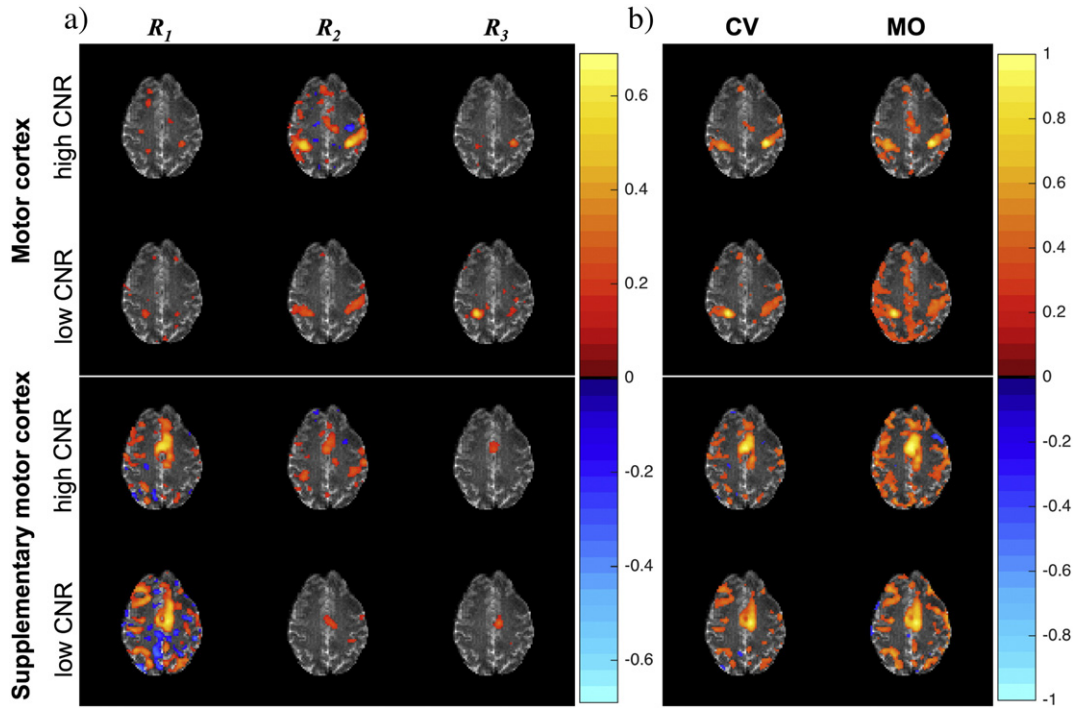

Fig. 3. Experimental MO fMRI spatial correlation maps for each seed voxel (a) by the correlation bands, R_1, R_2, R_3 corresponding to the frequency band ranges 0.0009–0.024 Hz, 0.026–0.037 Hz, 0.038–0.08 Hz, and (b) the total correlation map CV and MO for high and low CNR in motor cortex and supplementary motor cortex.

Fig. 4. Experimental CV fMRI spatial correlation maps for each seed voxel (a) by the correlation bands, R_1, R_2, R_3 corresponding to the frequency band ranges 0.0009–0.024 Hz, 0.026–0.037 Hz, 0.038–0.08 Hz, and (b) the total correlation map CV and MO for high and low CNR in motor cortex and supplementary motor cortex.

fMRI studies. In comparison to the MO correlations, the CV correlations have reduced error, and more distinctive regions of activation in the motor cortex and the supplementary motor cortex for voxels with lower magnitude and phase CNR. While the framework is demonstrated for task fMRI data, a natural application of this framework is to non-task fMRI, where the spatial correlation is measured to detect long-range connectivity.

The temporal Fourier frequency description in this study is also advantageous to locate the temporal frequency range where correlations are induced. Common processing and reconstruction methods have been shown to induce correlation of no biological origin [18,23,24]. In this study a framework is presented where signal processing operations and parallel image reconstruction procedures, applied to the complex-valued *k*-space signal, can be represented as real-valued matrix operators. The second order temporal frequency spatial covariance representation describes spatial correlation as a function of increased overlapping frequency content. Consider a scenario where initially voxel *a* and *b* are correlated, *b* and *c* are correlated, but *a* and *c* are not correlated. If the reconstructed images are smoothed, which have been previously shown to induce correlation, spatial correlation between *a* and *b* arises from overlapping frequency content between temporal frequency spectrums of *a* and *c*. Similar reasoning can be used to discuss the correlation between *b* and *c*, and the lack of correlation between *a* and *c*. As shown in Appendix A, the matrix multiplication of the linear operators with the spatial covariance matrix, quantitatively describes the compounding impact of spatial and temporal operators to the second order temporal frequencies. Combining this matrix multiplication framework with biologically or experimentally relevant frequency bands pertaining to fMRI data, provides insight into the impact of signal processing on statistical analysis and clinical interpretations from the data. The application of the theory to complex-valued data validates the increased statistical strength of using complex-valued models, specifically in minimally processed data sets or data sets with high noise variability. Including the phase

in the analysis increases the sensitivity of the correlation in low magnitude contrast-to-noise ratio functional MRI data.

Acknowledgements

Appendix A

A linear matrix representation of the spatial covariance and correlation, allows one to measure the effect of the temporal and spatial processing operators. Define a $p \times p$ spatial smoothing operator, S_m, which filters the real and imaginary components separately with a Gaussian kernel. Continuing the notation used in Eq. (3) with a demeaned time-series notation, the smoothed $2pn \times 1$ temporal frequency vector is constructed with the multiplication $v_s = (I_p \otimes \overline{\Omega}_T)P(I_{2n} \otimes S_m)y$.

The series of operations applied to the temporal frequencies is defined with $2pn \times 2pn$ operator,

$O = (I_{2n} \otimes S_m)P(I_p \otimes \overline{\Omega}_T)$ such that the $2pn \times 1$ unprocessed and processed time-series vectors ordered by voxel are represented as in Eqn. (3), $y = (I_p \otimes \overline{\Omega}_T)v$ and $y_s = Ov$. The $2pn \times 2pn$ spatiotemporal covariance matrix for the $2pn \times 1$ real-valued image time-series, y, in terms of temporal frequency spectrum, is defined as

$$cov[y] = \Gamma, \tag{A.1}$$

and the covariance matrix with processing operators is defined

$$cov[y_s] = O\Gamma O'. \tag{A.2}$$

Eqs. (A.1) and (A.2) are described in terms of temporal frequencies as shown in Section 2.1. The spatial component of Eq. (A.1) is equivalent to Σ described in Eq. (5), through a process of summing real and imaginary diagonal values to achieve a $sp \times p$

magnitude-squared spatial correlation matrix such that the temporal component is held constant. Magnitude-squared correlation is asymptotically equivalent to MO correlation [13,25].

References

[1] Bandettini PA, Wong EC, Hinks RS, Tikofsky RS, Hyde JS. Time course EPI of human brain function during task activation. Magn Reson Med 1992;25:390–7.

[2] Ogawa S, Lee TM, Kay AR, Tank DW. Brain magnetic resonance imaging with contrast dependent on blood oxygenation. Proc Natl Acad Sci U S A 1990;87:9868–72.

[3] Hoogenraad FG, Pouwels PJ, Hofman MB, Reichenbach JR, Sprenger M, Haacke EM. Quantitative differentiation between BOLD models in fMRI. Magn Reson Med 2001;45:233–46.

[4] Menon RS. Postacquisition suppression of large-vessel BOLD signals in high-resolution fMRI. Magn Reson Med 2002;47:1–9.

[5] Nencka AS, Rowe DB. Reducing the unwanted draining vein BOLD contribution in fMRI with statistical post-processing methods. Neuroimage 2007;37:177–88.

[6] Zhao F, Jin T, Wang P, Hu X, Kim SG. Sources of phase changes in BOLD and CBV-weighted fMRI. Magn Reson Med 2007;57:520–7.

[7] Feng Z, Caprihan A, Blagoev KB, Calhoun VD. Biophysical modeling of phase changes in BOLD fMRI. Neuroimage 2009;47(2):540–8.

[8] Rowe DB, Logan BR. A complex way to compute fMRI activation. Neuroimage 2004;23:1078–92.

[9] Rowe DB. Modeling both the magnitude and phase of complex-valued fMRI data. Neuroimage 2005;25:1310–24.

[10] Rowe DB. Magnitude and phase signal detection in complex-valued fMRI data. Magn Reson Med 2009;62:1356–7.

[11] Arja SK, Feng Z, Chen Z, Caprihan A, Kiehl KA, Adali T, et al. Changes in fMRI magnitude data and phase data observed in block-design and event-related tasks. Neuroimage 2010;49:3149–60.

[12] Cordes D, Haughton VM, Arfanakis K, Carew JD, Turski PA, Quigley MA, et al. Frequencies contributing to functional connectivity in the cerebral cortex in "resting-state" data. Am J Neuroradiol 2001;22:1326–33.

[13] Birn RM, Diamond JB, Smith MA, Bandettini PA. Separating respiratory-variation-related fluctuations from neuronal-activity-related fluctuations in fMRI. Neuroimage 2006;31:1536–48.

[14] Glover GH, Li TQ, Ress D. Image-based method for retrospective correction of physiological motion effects in fMRI: RETROICOR. Magn Reson Med 2000;44:162–7.

[15] Hahn AD, Nencka AS, Rowe DB. Enhancing the utility of complex-valued functional magnetic resonance imaging detection of neurobiological processes through post acquisition estimation and correction of dynamic B_0 errors and motion. Hum Brain Mapp 2012;33:288–306.

[16] Hu X, Le TH, Parrish T, Erhard P. Retrospective estimation and correction of physiological fluctuation in functional MRI. Magn Reson Med 1995;34:201–12.

[17] Friston KJ, Josephs O, Zarahan E, Holmes AP, Rouquette S, Poline JB. To smooth or not to smooth? Bias and efficiency in fMRI time-series analysis. Neuroimage 2000;12:196–208.

[18] Nencka AS, Hahn AD, Rowe DB. A mathematical model for understanding statistical effects of k-space (AMMUST-k) preprocessing on observed voxel measurements in fcMRI and fMRI. J Neurosci Methods 2009;181:268–82.

[19] Davey CE, Grayden DB, Egan GF, Johnston LA. Filtering induces correlation in fMRI resting state data. Neuroimage 2013;64:728–40.

[20] Bhattacharyya PK, Lowe MJ. Cardiac-induced physiologic noise in the tissue is a direct observation of cardiac-induced fluctuations. Magn Reson Imaging 2004;22:9–13.

[21] Shmueli K, van Glederen P, de Zwart JA, Horovitz SG, Fukunaga M, Jansma JM, et al. Low-frequency fluctuation in the cardiac rate as a source of variance in the resting-state fMRI BOLD signal. Neuroimage 2007;38:306–20.

[22] Rowe DB, Nencka AS, Hoffmann RG. Signal and noise of Fourier reconstructed fMRI data. J Neurosci Methods 2007;159:361–9.

[23] Bruce IP, Karaman MM, Rowe DB. A statistical examination of the SENSE reconstruction via an isomorphism representation. Magn Reson Imaging 2011;29:1267–87.

[24] Bruce IP, Rowe DB. Quantifying the statistical impact of GRAPPA in fcMRI data with a real-valued isomorphism. IEEE Trans Med Imaging 2014;33:495–503.

[25] Rowe DB, Nencka AS. Induced correlation In FMRI magnitude data from k-space preprocessing. Proc Int Soc Magn Reson Med 2009;17:1721.